

Application of a data-assimilation model to variability of Pacific sardine spawning and survivor habitats with ENSO in the California Current System

Hajoon Song,¹ Arthur J. Miller,² Sam McClatchie,³ Edward D. Weber,³ Karen M. Nieto,³ and David M. Checkley Jr.²

Received 19 May 2011; revised 6 January 2012; accepted 7 January 2012; published 8 March 2012.

[1] The Pacific sardine (*Sardinops sagax*) showed significant differences in spawning habitat area, spawning habitat quality and availability of survivor habitat as the Pacific Ocean went through the La Niña state in April 2002 to a weak El Niño in April 2003. During another El Niño/Southern Oscillation transition period in 2006–2007 when the El Niño state retreated and the La Niña returned, a similar pattern in spawning habitat quality was seen. The coupling between the atmospheric forcing, the physical ocean states and the properties of the sardine egg spawning are investigated using dynamically consistent data-assimilation fits of the available physical oceanographic observations during these months. Fits were executed using the Regional Ocean Modeling System four-dimensional variational assimilation platform along with adjoint model runs using a passive tracer to deduce source waters for the areas of interest. Analysis using the data-assimilation model runs reveals that unusually strong equatorward wind-forcing drives offshore transport during the La Niña conditions, which extends the spawning habitat for sardine further offshore. A statistical model of sardine spawning habitat shows better habitat quality during the El Niño conditions, which is associated with higher egg densities and corresponded to higher daily egg production. Concentration of eggs is also increased by convergence of water. The results of the source waters analysis using the adjoint data assimilation model support the idea that offshore transport extends the spawning habitat, and show that higher levels of nutrient are brought into the spawning habitat with high concentration of sardine eggs.

Citation: Song, H., A. J. Miller, S. McClatchie, E. D. Weber, K. M. Nieto, and D. M. Checkley Jr. (2012), Application of a data-assimilation model to variability of Pacific sardine spawning and survivor habitats with ENSO in the California Current System, *J. Geophys. Res.*, 117, C03009, doi:10.1029/2011JC007302.

1. Introduction

[2] The California Current System (CCS), which is one of the most studied eastern boundary currents, is characterized as an active upwelling and biologically productive region, providing a good habitat for small pelagic fish. The California Current ecosystem is influenced by environmental variations on various timescales through effects of solar flux, oceanic temperature, lateral advection, vertical mixing and upwelling [Miller *et al.*, 2004; Checkley and Barth, 2009].

[3] The Pacific sardine (*Sardinops sagax*), which is a key commercial species supporting fisheries landing of 90,492 mt (averaged from 2005–2009) is strongly affected

by environmental variability. From the rich time series of the California Cooperative Oceanic Fisheries Investigations (CalCOFI) program, it is well known that the spawning biomass and spawning habitat of sardine varies considerably between years [Lo *et al.*, 2005; Reiss *et al.*, 2008; Weber and McClatchie, 2010]. Among climatological variations, El Niño/Southern Oscillation (ENSO) events on interannual time-scales alters the ecosystem significantly in the CCS [Miller *et al.*, 2004]. For example, the area of the spawning habitat, based on the egg distributions, increased by an order of magnitude during the transition from the 1998 El Niño to the 1999 La Niña [Reiss *et al.*, 2008]. However, daily egg production was higher in 1998 than in 1999 [Bjorkstedt *et al.*, 2010]. The strongest contrast between sardine egg densities across an ENSO transition in the entire time series of the high resolution egg data (1997–2011) was observed from the 2002 La Niña (lower daily egg production but greater spawning habitat area) to the 2003 El Niño conditions (with higher daily egg production but smaller spawning habitat area) [Bjorkstedt *et al.*, 2010]. However, ENSO does not always drive a big contrast in sardine egg abundance. During the

¹Department of Ocean Sciences, University of California, Santa Cruz, California, USA.

²Scripps Institution of Oceanography, University of California, San Diego, La Jolla, California, USA.

³Southwest Fisheries Science Center, NOAA, La Jolla, California, USA.

2006 El Niño and 2007 La Niña, the ocean states showed significant differences, but densities of Pacific sardine eggs were not as dramatically different compared to the 2002–2003 ENSO transition.

[4] When the CCS was under the influence of La Niña in April 2002 (0204LN) and 2007 (0704LN), it had stronger than normal equatorward wind. Thus the CCS had stronger upwelling than average, causing a negative sea surface temperature (SST) anomaly [Schwing *et al.*, 2002b; Peterson *et al.*, 2006; Goericke *et al.*, 2007]. When the CCS was under the influences of the Central Pacific El Niño in April 2003 (0304EN) and 2006 (0604EN) [Goericke *et al.*, 2007; Singh *et al.*, 2011], the wind patterns over the North Pacific were anomalously cyclonic, which caused weaker than normal equatorward wind over the CCS. As a result of weaker upwelling than average, 0304EN and 0604EN showed a warm SST anomaly [Venrick *et al.*, 2003; Goericke *et al.*, 2007].

[5] Although large-scale features associated with ENSO variations provide intuition about the coupling between the physical ocean states and the sardine eggs distributions, better understanding about the link is often inhibited by a lack of information about the oceanic states with mesoscale or smaller features. Numerical ocean models can provide oceanic fields with small scale features, but they may diverge from the observed oceanic states and not be adequate to interpret the responses of the ecosystem to the physical oceanic changes in that case. Field and satellite observations provide important information about the systems, but they have limited temporal and spatial coverage.

[6] Data assimilation is a technique that combines observations and models to determine the best possible estimate of the state of a dynamical system [Ghil and Malanotte-Rizzoli, 1991]. The variational method represents one of two groups in data assimilation methodologies, and it is based on optimal control theory which seeks the model trajectory that best fits the data over a given period of time [Le Dimet and Talagrand, 1986]. The variational method is employed in this study to combine observations of sea surface height (SSH), SST, and hydrographic temperature (T) and salinity (S) data, with a physical ocean model. The solutions are then used to diagnose the mechanisms behind the observed variations in the sardine egg sampling data.

[7] In this paper, the physical forcing mechanisms responsible for the observed changes in the Pacific sardine egg distributions are examined based on the following hypotheses. Wind-forcing affects the horizontal sardine egg distributions by changing preferred spawning habitat. Spawning habitat quality can be partially explained by physical properties such as temperature, salinity and convergence of water, as well as the biological properties of source waters. Mesoscale eddies are one of the possible mechanisms to determine the survival of sardine egg and larvae. To test these hypotheses, data from ship-board surveys, satellite remote sensing, a statistical model of sardine spawning habitat [Weber and McClatchie, 2010] and a physical model of data-assimilated ocean states are used. Then the analyses link sardine egg distributions to atmospheric forcing, oceanic states, characteristics of water sources, and mesoscale features thought to be important for sardine larval growth and survival.

[8] The focus of this paper is to demonstrate how a data assimilation model and adjoint analysis can lead to better

understanding of the effects of physical forcing on sardine spawning habitat. The analysis includes not only variables that have been widely studied such as SST and upwelling [Checkley *et al.*, 2000; Reiss *et al.*, 2008], but also variables that need to be computed such as transport and velocity potential. The analysis is further extended with a sensitivity computation using an adjoint model for the diagnosis of source waters.

[9] The remainder of the paper is organized as follows. Section 1 discusses the biological and physical oceanographic data used in data assimilation. Then section 3 describes the details of the physical model setting and gives a short description of the data assimilation system and the adjoint model. The statistical model for sardine habitat is also briefly described. Discussion of the horizontal distribution of sardine eggs, quality of sardine spawning habitat, availability of larval survivor habitat, and source waters for the spawning areas are presented in sections 4, 5, 6, and 7, respectively. Then a summary and a discussion are presented in section 8.

2. Field and Satellite Observations

2.1. Biological Observations

[10] Since 1997, fine scale Pacific sardine egg monitoring has become routinely available using Continuous Underway Fish Egg Sampler (CUFES) [Checkley *et al.*, 1997, 2000]. CUFES samples pelagic fish eggs continuously at 3 m depth, providing densities of selected species of fish eggs every 15–30 minutes along the vessel track that can be used to study the sardine spawning habitat. CUFES stations in 0204LN, 0304EN, 0604EN and 0704LN in Figures 1a–1d, covered the Southern California Bight (SCB) and central California.

[11] The sampled sardine eggs in Figures 1e–1h show variations in horizontal distribution. In 0204LN, sardine eggs extended far offshore except in areas to the south of 31°N. Densities near the coast and offshore from the SCB were low. While the density of eggs far offshore from the SCB was low in 0204LN, sardine eggs were absent far offshore of the SCB and Point Conception in 0304EN, highlighting the greater offshore extent of eggs during 0204LN. However, the total number of eggs was greater, and egg densities were higher, in 0304EN. There were no stations with observed sardine eggs greater than 100 eggs m⁻³ in 0204LN, but 10 stations in 0304EN contained eggs exceeding 100 eggs m⁻³. In 0304EN, the total egg count was 45207, which was more than twice the number of eggs in 0204LN. In both periods, the stations that were offshore of Point Conception or to the north showed higher numbers of sampled eggs. In 0604EN and 0704LN, sardine eggs were sampled at most of CUFES stations. However, unlike previous years, highest densities of sardine eggs were concentrated to the south of Point Conception in both 0604EN and 0704LN. A couple of stations offshore of the SCB showed egg concentrations higher than 100 eggs m⁻³ in 0604EN. In 0704LN, the concentration of the sampled sardine eggs was not as abundant as previous years [McClatchie *et al.*, 2008].

[12] Monthly averaged near-surface chlorophyll-*a* (Chl-*a*) data were obtained from the NASA Sea-viewing Wide Field-of-View Sensor (SeaWiFS, <http://seawifs.gsfc.nasa.gov>) for 0204LN, 0304EN, 0604EN and 0704LN, and plotted on a logarithmic scale in Figures 2a–2d. The spawning habitat model of Weber and McClatchie [2010]

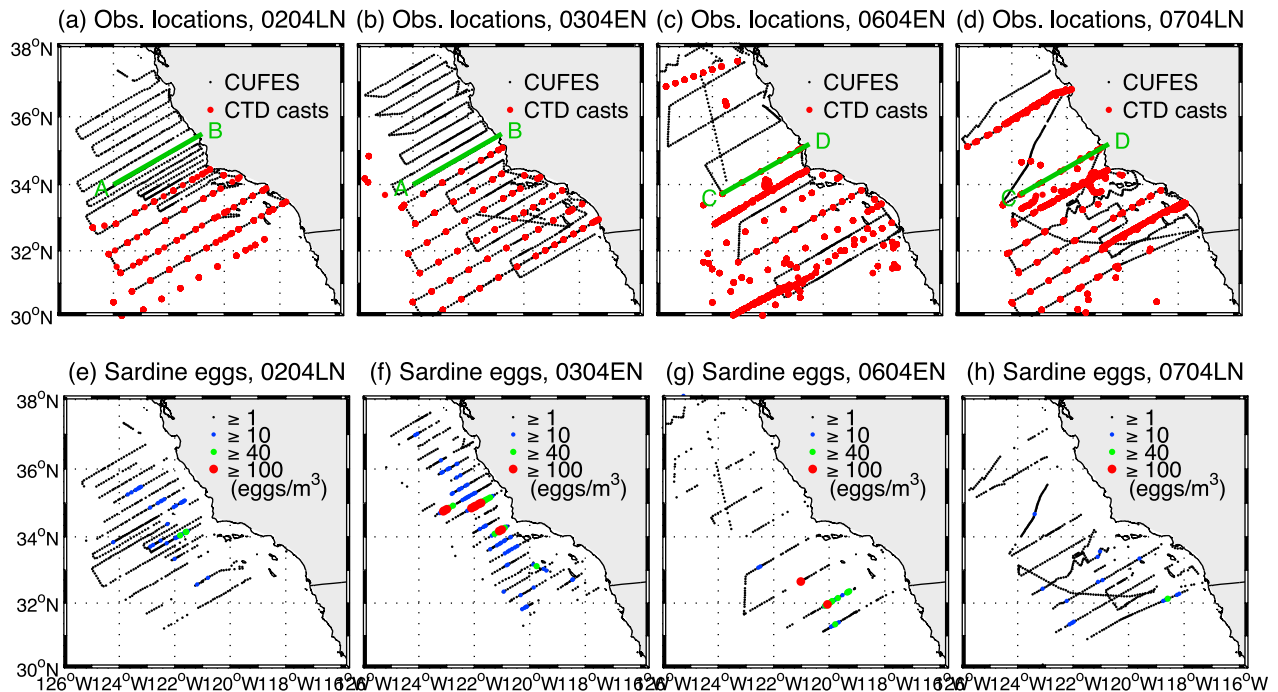


Figure 1. CUFES stations and subsurface observation locations used in the data assimilation for (a) 0204LN (2002 April), (b) 0304EN (2003 April), (c) 0604EN (2006 April) and (d) 0704LN (2007 April), and densities of Pacific sardine eggs at each CUFES station in (e) 0204LN, (f) 0304EN, (g) 0604EN and (h) 0704LN. In Figures 1e–1h, black dots represent the CUFES station that sampled at least one sardine egg. Blue, green and red dots represent the CUFES station that sampled the sardine eggs with densities greater than 10, 40 and 100 eggs/m^3 , respectively. The solid green lines A–B in Figures 1a and 1b and C–D in Figures 1c and 1d indicate the transects for density vertical section shown in Figure 7.

indicates that the probability for capturing eggs is a convex parabolic function of Chl-*a* concentrations at median levels of temperature and salinity. Unlike anchovy, sardine does not spawn in areas with bloom concentrations of phytoplankton. Figures 2a–2d show that the stations with high egg concentration are generally associated with mid-range Chl-*a* concentration ($0.5 \sim 1.75 \text{ mg m}^{-3}$).

2.2. Physical Observations

[13] Data assimilation is used to fit various data sets including satellite and *in situ* observations in the experiments. The satellite observations are the SST data from the 4 km resolution advanced Very-High-Resolution Radiometers (AVHRR) and along-track SSH anomaly data produced by Ssalto/Duacs and distributed by AVISO. *In situ* observations are hydrographic T and S from CalCOFI program CTD casts and near surface (–3 m) T and S from CUFES surveys for all assimilation periods. Argo profiles are used for 0304EN, 0604EN and 0704LN assimilation. For 0604EN and 0704LN, underwater Spray gliders provides T and S with high horizontal resolution data from the surface down to –500 m [Sherman *et al.*, 2001]. For 0704LN, the California Current Ecosystem Long Term Ecological Research (CCE LTER) cruise provides T and S near Point Conception (<http://cce.lternet.edu/data/>). The location of all *in situ* observations are shown with red dots in Figures 1a–1d. The observation type and the availability are summarized in Table 1.

[14] Remotely sensed data from AVHRR in Figures 2e–2h show the SST and upwelling patterns. When the La Niña influenced the CCS (Figures 2e and 2h), the SST was generally colder than when the CCS was under the influence of the Central Pacific El Niño (Figures 2f and 2g) [Schwing *et al.*, 2002b; Venrick *et al.*, 2003; Peterson *et al.*, 2006; Goericke *et al.*, 2007]. Coastal upwelling was apparent in the coastal areas to the north of Point Conception in 0204LN, 0304EN and 0704LN where the SST was below 12°C. However, the coastal upwelling was weak or absent in 0604EN. This is because the onset of seasonal upwelling was delayed up to two months compared to usual years [Schwing *et al.*, 2006]. In contrast, anomalously strong coastal upwelling began early in 2007 [Goericke *et al.*, 2007].

3. Model

3.1. Physical Ocean Model and Data Assimilation

[15] In this experiment, the Regional Ocean Modeling System (ROMS) four-dimensional variational data assimilation (4DVAR) system [Moore *et al.*, 2011] was used to estimate the ocean states. The model domain covers 30°N to 38°N and 115.7°W to 126°W with an approximately 9 km grid interval. It has 42 terrain-following vertical levels that are concentrated more at the surface and ocean bottom. Background initial and boundary conditions were extracted from the data-assimilation data set developed by Broquet

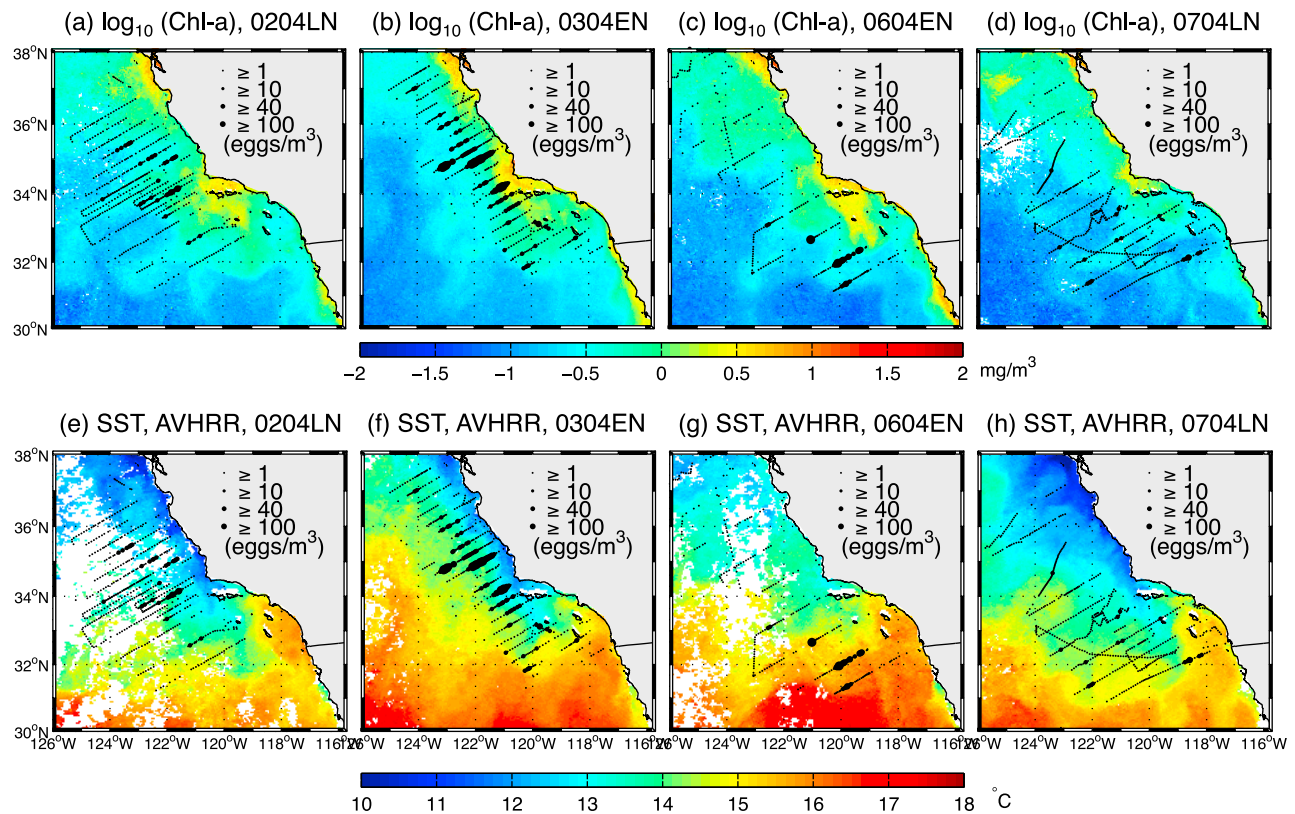


Figure 2. Monthly mean surface chlorophyll-*a* from SeaWiFS for (a) 0204LN, (b) 0304EN, (c) 0604EN and (d) 0704LN in \log_{10} scale, and monthly mean SST from AVHRR for (e) 0204LN, (f) 0304EN, (g) 0604EN and (h) 0704LN. White gaps show the areas with bad data quality. Pacific sardine egg distributions are plotted with black dots, and size of dots represent the egg densities.

et al. [2009], and the surface boundary conditions were obtained from prior model solutions of the 9 km resolution Coupled Ocean/Atmosphere Mesoscale Prediction System (COAMPS[®]) [Hodur *et al.*, 2002; Doyle *et al.*, 2009] using bulk formulation [Fairall *et al.*, 1996].

[16] The ROMS 4DVAR collects observations over a defined assimilation time window and is able to adjust the initial condition, surface forcing, boundary condition and model itself with given errors to reduce the misfit between the model and the observations. In the experiments, data assimilation was performed using the data sets described in section 2.2. The fit was achieved by adjusting the initial condition and surface forcing to allow the model simulation to fit the observed data in a least square sense. The adjustment of surface forcing was computed using the model dynamics and prescribed errors. The adjoint model interprets the misfits to the surface forcing adjustment using the model dynamics. Then the adjustment is scaled by the errors in the surface forcing, which results in the surface forcing adjustment. If only the initial condition is adjusted, information from the observations can be diminished with a long run. Thus adjusting surface forcing allows the model to keep tracking the observed states more accurately over the time periods of these fits.

[17] The data set generated by Broquet *et al.* [2009] is already a fit to observations using the same data assimilation

machinery, but with 7 days assimilation time window. It can cause dynamical inconsistency every 7 days when the initial conditions are re-set, which can generate gravity waves. In the experiments, the assimilation window was set to one month, which guarantees dynamically balanced ocean states for the experiment time period. Also the observations used in the data assimilation experiment are different from the data set by Broquet *et al.* [2009]. Instead of gridded satellite SSH data and COAMPS[®] SST data that were used in their data set, along-track satellite sea level height data and the SST data were assimilated in the current study.

Table 1. Data Set Used in the Data Assimilation With the Observation Type (Obs. Type) and the Availability^a

Data Set	Obs. Type	Availability			
		0204LN	0304EN	0604EN	0704LN
AVHRR	SST	X	X	X	X
AVISO	SSH	X	X	X	X
CUFES	T, S (-3 m)	X	X	X	X
CalCOFI	T, S (>-500 m)	X	X	X	X
Argo	T, S (>-2000 m)		X	X	X
Glider	T, S (>-500 m)			X	X
CCE LTER	T, S (>-940 m)				X

^aThe crosses indicate the availability of the data set at each period.

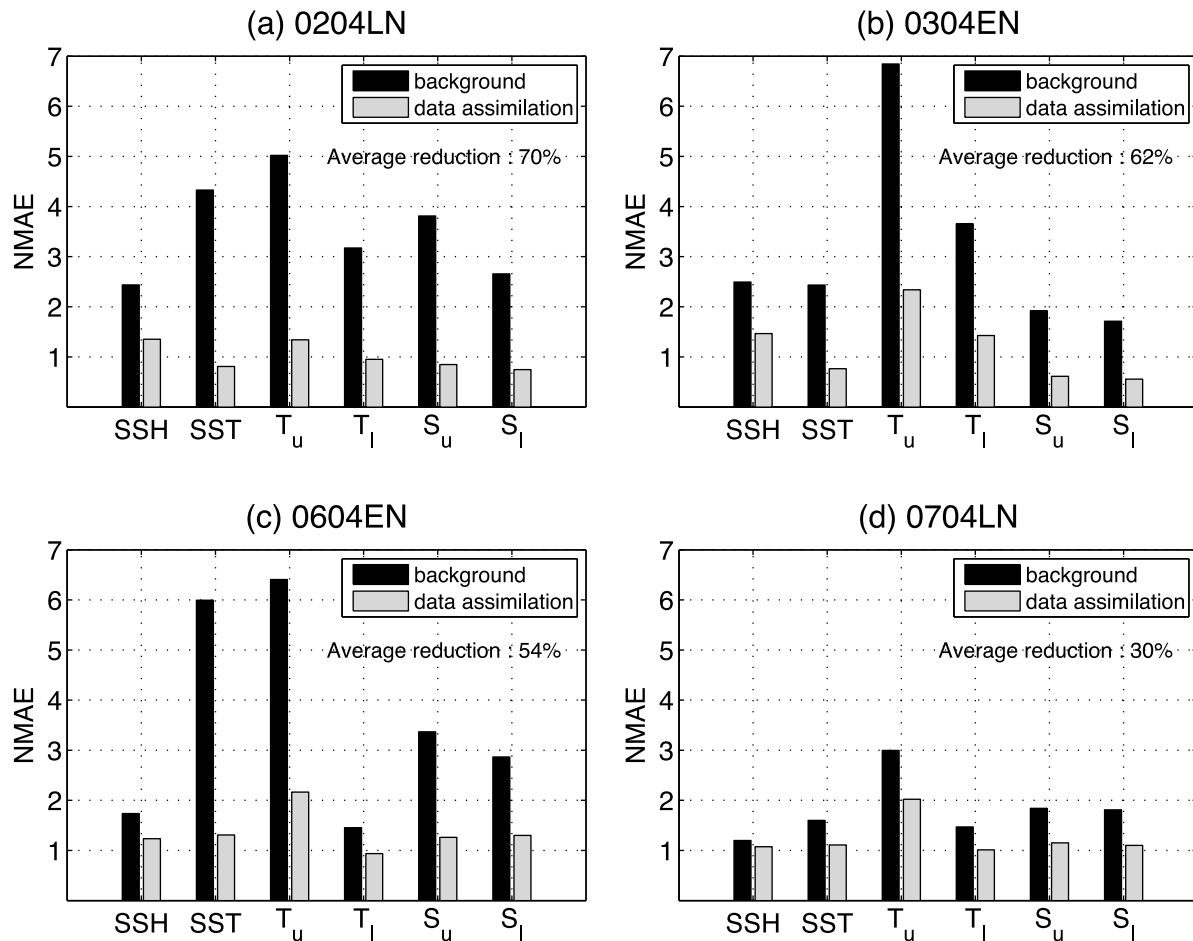


Figure 3. Normalized mean absolute error changes in (a) 0204LN, (b) 0304EN, (c) 0604EN and (d) 0704LN for sea surface height (SSH), sea surface temperature (SST), temperature in upper -100 m (T_u), temperature below -100 m (T_l), salinity in upper -100 m (S_u) and salinity below -100 m (S_l).

[18] The 4DVAR in most realistic atmospheric and oceanic models uses iterative methods to find the optimal states because the size of dimension often prohibits the matrix inverse calculation that appears in the optimal solution. In these experiments, a total of 45 iterations were used, and this was adequate for the convergence of the solutions. Figure 3 shows the reduction of the normalized mean absolute error (NMAE) for 0204LN, 0304EN, 0604EN and 0704LN. If the NMAE is one, it means the misfit between the observations and the interpolated model states is the same as the observational error on average. In 0204LN, the NMAE became roughly one after ROMS 4DVAR system decreased the normalized misfit by 70% on average. The NMAE in 0304EN is approximately 1.4 after the 62% reduction on average. The decreases in mean NMAE for 0604EN and 0704LN are 54% and 30%, respectively. Song [2011] provides the details about the data assimilation experiment setup and results.

[19] A one-month run of the ROMS adjoint model was also used to track the water sources for the areas of interest. The adjoint model computes the sensitivity of a defined scalar quantity, J , to model variables at every grid point over time. If J is defined as passive tracer concentration, the adjoint model runs backward in time and computes the sensitivity to the model variables. In the absence of sources

or sinks, the adjoint model result with passive tracer J can be interpreted as the water sources [Fukumori *et al.*, 2004; Chhak and Di Lorenzo, 2007; Song *et al.*, 2011]. The adjoint model can further quantify the contribution of the source waters to the areas of interest.

3.2. Sardine Spawning Habitat Model

[20] The statistical spawning habitat model of Weber and McClatchie [2010] was used to estimate the probability of occurrence of sardine eggs over the spatial domain where the relevant environmental data were present in 0204LN, 0304EN, 0604EN and 0704LN. Briefly, the model is a constrained logistic Generalized Additive Model using mean temperature, salinity and chlorophyll in the upper 50 m, and sardine stock size in the preceding year, to predict the probability of occurrence of sardine eggs. The probability of occurrence of sardine eggs is interpreted as a measure of spawning habitat quality. The model was run with ship-collected survey data from the 6 core CalCOFI transects between San Diego and Avila Beach, California, and was used to make approximate predictions with data from the ROMS model for the broader spatial domain. For the ROMS model, the chlorophyll predictor was estimated from a regression relation between SeaWiFS satellite data within

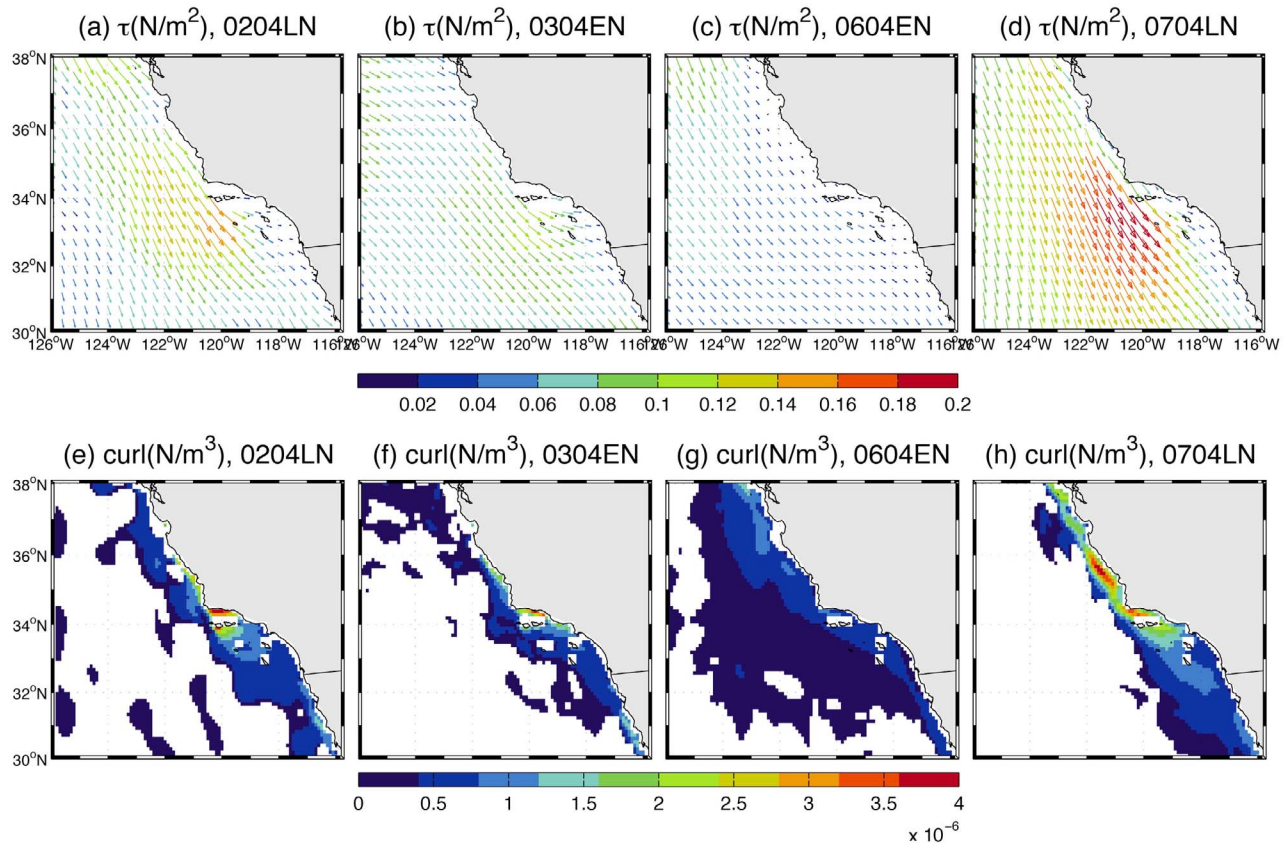


Figure 4. (a–d) Wind stress and (e–h) wind stress curl averaged over 0204LN (Figures 4a and 4e), 0304EN (Figures 4b and 4f), 0604EN (Figures 4c and 4g) and 0704LN (Figures 4d and 4h) after data assimilation. In Figures 4e–4h, only positive values of wind stress curl are plotted in order to indicate the areas of upwelling by Ekman pumping.

12 km of CalCOFI stations where chlorophyll was measured in the upper 50 m ($R^2 = 0.68$, $n = 127$).

4. Horizontal Distribution of Eggs

4.1. Wind-Forcing and Surface Current

[21] As a result of an anomalously strong North Pacific High in 2002 and 2007, upwelling-favorable wind became stronger than normal over the CCS in 0204LN and 0704LN. In 0304EN and 0604EN, an unusually weak North Pacific High drove the upwelling-favorable wind to be weaker than normal over the CCS. This is shown in Figure 4, which plots the wind stress (Figures 4a–4d) and wind stress curl (Figures 4e–4h) during 0204LN, 0304EN, 0604EN and 0704LN after the ROMS 4DVAR system adjusted the COAMPS[®] wind-forcing. The direction of the wind stress is equatorward along the coast in all periods, but the intensity of the wind stress varies. The wind stress is generally stronger when the CCS is under the influence of La Niña (0204LN and 0704LN) than when it is under the influence of El Niño (0304EN and 0604EN). The strongest wind stress is found in 0704LN, and the weakest wind stress was found in 0604EN.

[22] In Figures 4e–4h, only the positive values of the wind stress curl are plotted in order to indicate the areas with upwelling by Ekman pumping. The highest contrast in the

wind stress curl is found for 0604EN and 0704LN. In 0604EN, positive wind stress curl is observed over broad areas in the CCS with small magnitude ($<1.5 \times 10^{-6} \text{ N m}^{-3}$). In contrast, positive wind stress curl with high magnitude ($>3 \times 10^{-6} \text{ N m}^{-3}$) is found over a narrow band at the coast in 0704LN. The wind stress curl in 0204LN is positive over broader areas between Point Conception and Monterey Bay with higher intensity near Point Conception compared to 0304EN.

[23] Equatorward wind drives offshore transport through Ekman transport in the CCS. The offshore transport is positively proportional to the equatorward wind stress, hence one can expect that anomalous upwelling favorable wind drives more offshore transport. The surface current in Figure 5 can partially explain the features seen in the egg distribution. In 0204LN, the surface current flows in the offshore direction at 124°W and 34°N , where the offshore CUFES stations sampled sardine eggs. This flow can carry the upwelled water to the offshore in 0204LN. In 0304EN, however, the main feature of the surface current is equatorward flow parallel to the coastline, and its location roughly coincides with the offshore edge of the sardine eggs distribution.

[25] The averaged offshore transports in the upper 30 m across the black line (approximately 300 km from the coast) in Figure 5 for 0204LN, 0304EN, 0604EN and 0704LN are $-1.2 \times 10^{-3} \text{ Sv}$, $-0.7 \times 10^{-3} \text{ Sv}$, $-0.6 \times 10^{-3} \text{ Sv}$

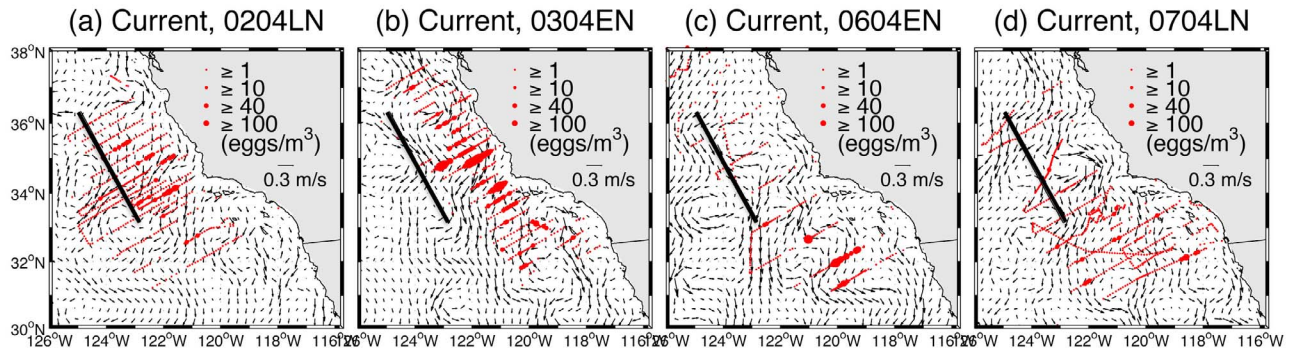


Figure 5. Pacific sardine eggs distribution and the surface current in (a) 0204LN, (b) 0304EN, (c) 0604EN and (d) 0704LN. The magnitude of the surface current is shown with color so that the darker the arrow is, the stronger the current is. The size of red dots represent the concentration of the sampled sardine eggs. Black lines represent the section for the cross-shore transport.

and -1.5×10^{-3} Sv, respectively. (Negative value represents offshore direction.) Thus, anomalous upwelling favorable wind during La Niña conditions results in more offshore transport, and the upwelled nutrient-rich water can be transported further offshore providing a good spawning habitat for Pacific sardine. The offshore transport, however, cannot be directly responsible for the horizontal distribution of eggs. Eggs are usually hatched in 72–96 hours after spawning in $12 \sim 14^\circ\text{C}$ water [Lo *et al.*, 1996], so they can travel less than 70 km within a 0.2 m s^{-1} current. For comparison, the offshore CalCOFI stations are about 74 km apart. From this it is inferred that what was observed is the result of stronger offshore transport in La Niña conditions moving the spawning habitat offshore rather than just moving the eggs. The wind moves the eggs, but they are present only for a short time and so the greater movement is due to a shift in the favorable spawning habitat for the adult fish.

4.2. Water Temperature

[26] As addressed by Reiss *et al.* [2008], the Pacific sardine spawning habitat is strongly influenced by the SST field. Figure 6 shows the data-assimilated SST and Pacific sardine egg distribution. In general, the SST from the ROMS data assimilation system shows a good agreement in pattern

and scale to the observed SST in Figures 2e–2h, except that the model SST at the coast of central California in 0204LN is warmer than the satellite observation meaning weaker upwelling in the model. This can be explained because data assimilation finds the dynamically consistent ocean states based on the given errors, which implies that the data assimilation solution will not perfectly match the observations.

[27] Monthly averaged SST in 0204LN, 0304EN, 0604EN and 0704LN are 13.65°C , 14.41°C , 14.16°C and 13.30°C , respectively, showing colder SST under the La Niña state. Although SST can be affected by the surface properties such as heat flux, colder SST is mainly due to more upwelling in 0204LN and 0704LN as the higher salinity values are measured in 0204LN and 0704LN CUFES stations than 0304EN and 0604EN (not shown). Since the offshore transport is stronger in 0204LN and 0704LN than other periods, upwelled water can be transported further offshore, resulting in gradual cross-shore SST changes. In contrast, the SST in 0304EN shows a pattern parallel to the coastline, which can be interpreted as an evidence of weaker offshore transport. The mean SST in 0604EN is colder than in 0304EN, and the SST gradient is weaker in cross-shore direction comparing to 0304EN, even if the offshore transport is the weakest in 0604EN. One of the possible explanations is that the positive

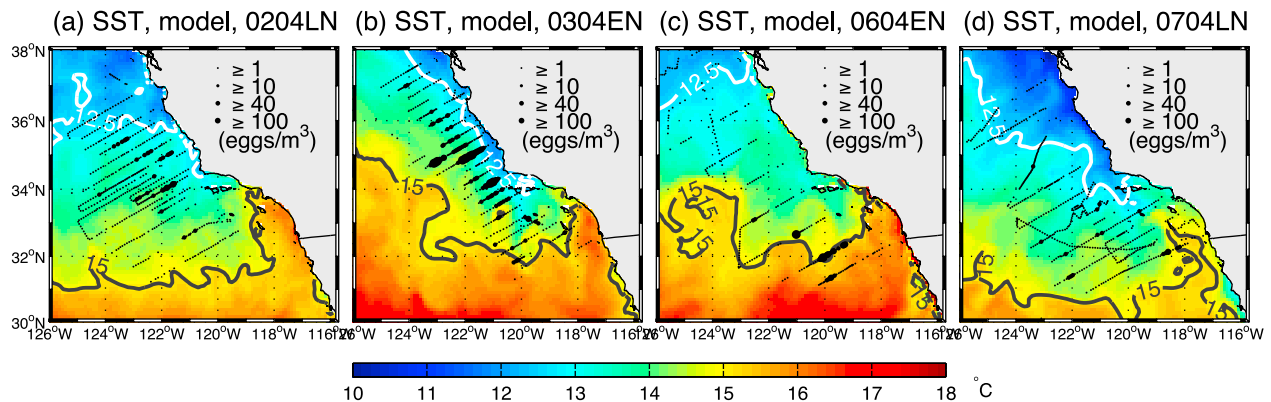


Figure 6. Pacific sardine eggs distribution over the SST from the data assimilated model in (a) 0204LN, (b) 0304EN, (c) 0604EN and (d) 0704LN. White and black contour lines represent 12.5 and 15°C isotherms.

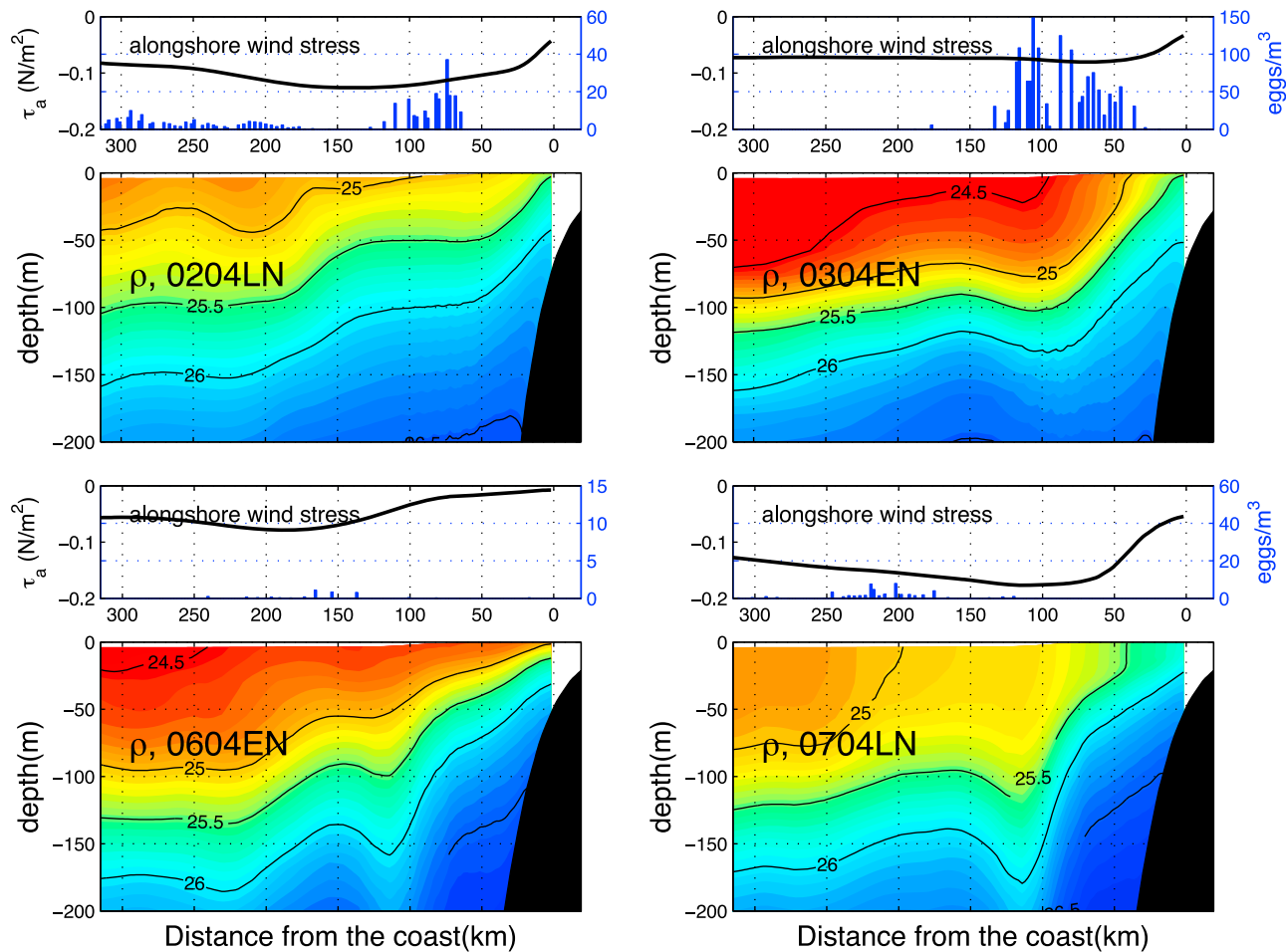


Figure 7. Alongshore wind stress (black solid lines), sardine egg counts (blue bar) and density (filled contour) from the surface to $-200m$ depth along the section A–B in Figure 1 for 0204LN and 0304EN, and along the section C–D for 0604EN and 0704LN. The values for wind stress are negative, meaning equatorward, and the egg counts are plotted with different scale. Areas with positive wind stress curl are indicated with red, though the saturation of the color does not represent the degree.

wind stress curl covering broad areas in 0604EN (Figure 4g) pumps up the subsurface water, which can cool down the SST in the open ocean.

[28] Figure 7 clearly shows the positive correlation between the wind stress at the coast and the coastal upwelling. The coastal upwelling is the strongest in 0704LN when the isopycnal of 25.5 outcrops about 50 km from the coast. The coastal upwelling in 0204LN and 0304EN is comparable when the wind stresses at the coast are similar, and 0604EN shows the weakest coastal upwelling.

[29] The sampled sardine egg data agree well with what *Checkley et al.* [2000] report. They characterize the spawning habitat of the Pacific sardine as a transition zone from the newly upwelled water near the coast to the California Current offshore. The isopycnal of 25 outcrops at about 100 km offshore in 0204LN, while it outcrops at less than 50 km from the coast in 0304EN. This indicates that newly upwelled water occupies broader areas near the coast in 0204LN than in 0304EN although their coastal upwellings are comparable. The areas with newly upwelled water are even broader in 0704LN when the 25 isopycnal outcrops 200 km

from the coast. Accordingly, the width of areas with no sampled sardine eggs from the coast is the largest in 0704LN, followed by 0204LN and 0304EN. The 0604EN is excluded here because so few eggs were sampled (<2 $eggs\ m^{-3}$).

[30] Vertical sections also show the open water upwelling by positive wind stress curl. Areas of positive wind stress curl induce the open water upwelling indicated by the lift of isopycnals. Combined with the coastal wind stress, the strongest positive wind stress curl near the coast in 0704LN caused the water density to be the greatest. Positive curl is found over the region from the coast to about 200 km offshore in 0604EN. As a result, denser water is found offshore near the surface in 0604EN compared to 0304EN, though the coastal upwelling is weaker. Although the wind stress at the coast is comparable in 0204LN and 0304EN, offshore wind stress curl changes the density features. In 0204LN, positive wind stress curl occurs from the coast to nearly 150 km offshore, forcing the surface water to diverge and inducing open-ocean upwelling. In contrast, the positive wind stress curl is seen only from the coast to 70 km offshore in 0304EN.

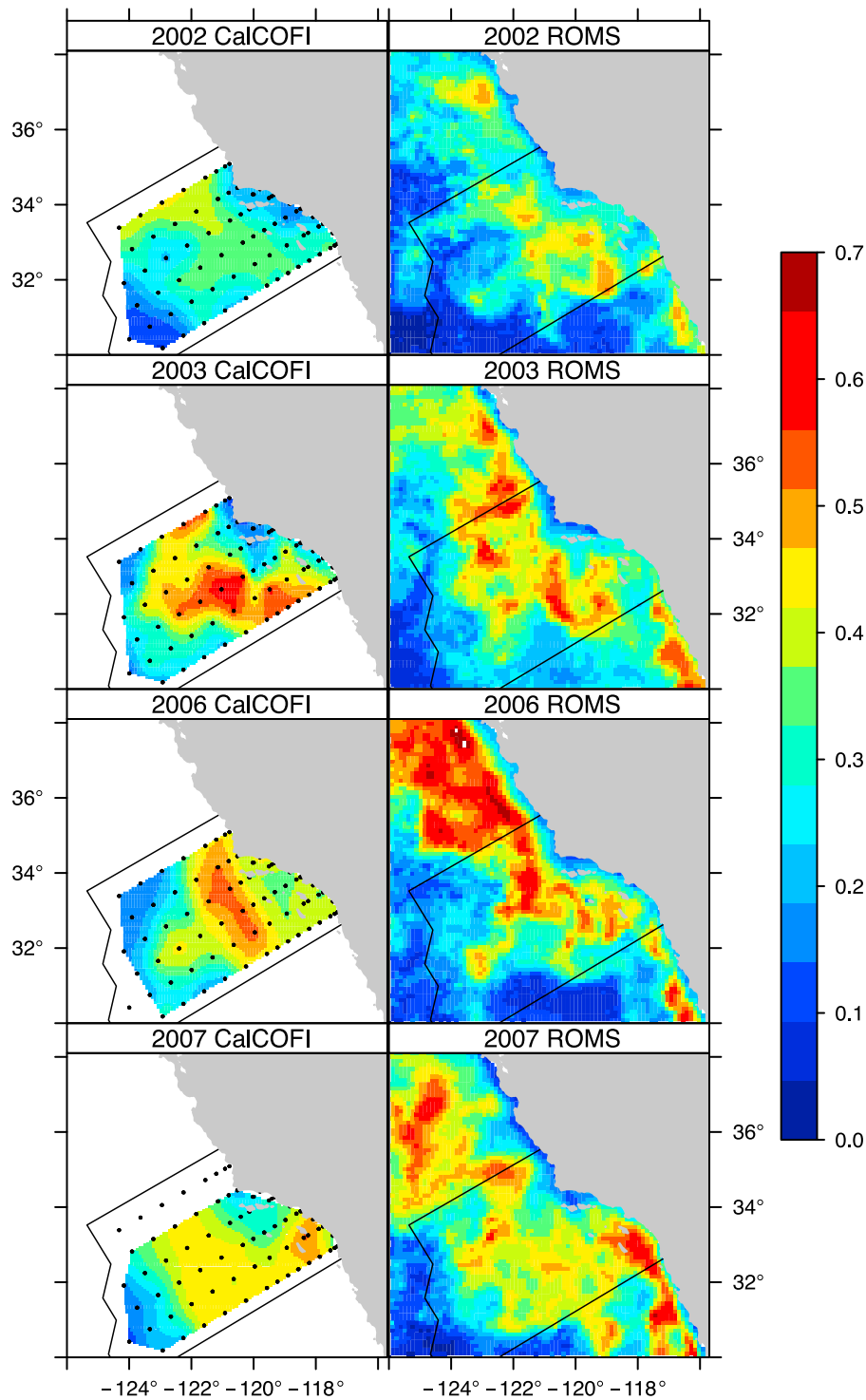


Figure 8. Statistical model predicting the probability of occurrence (0.0–1.0) of Pacific sardine eggs in 0204LN, 0304EN, 0604EN and 0704LN which is interpreted as a measure of sardine spawning habitat quality. (left) Generated using data from 6 core transects of the CalCOFI surveys as predictors (black dots show station positions). (right) Environmental variables from the ROMS model were used as predictors in the statistical model. Red areas indicate the highest quality sardine habitat.

[31] The size of spawning habitat appears to be related to both wind stress and wind stress curl. Open ocean upwelling is capable of bringing nutrients close to the surface which can supply plankters to sardine [Ryckaczewski and Checkley,

2008]. Thus the water offshore becomes nutrient-rich. Then, the offshore transport forced by equatorward wind stress can carry nutrient-rich water even further offshore. This is clearly seen in 0204LN and 0304EN sardine egg data. In

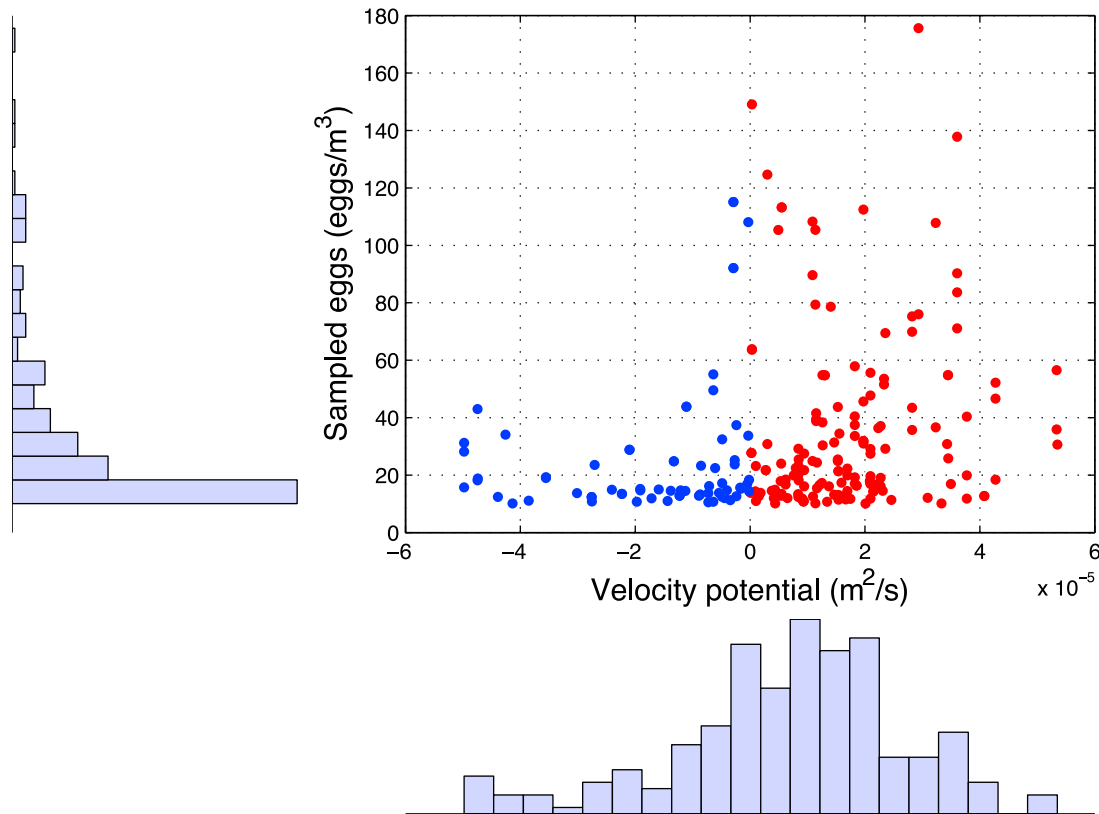


Figure 9. (top right) Scatterplot of sampled eggs and velocity potential, and their histograms. The CUFES stations with more than 10 eggs m^{-3} are selected from all periods, and velocity potential is averaged over the areas around the station within radius 0.3° . Red (blue) dots represent the points with positive (negative) velocity potential that is related to convergence (divergence). Histograms for (top left) sample eggs and (bottom) velocity potential.

0204LN, the equatorward wind stress offshore was greater than in 0304EN, and positive wind stress curl covers broader areas. The size of spawning habitat in 0204LN was broader, supporting the idea that both wind stress and wind stress curl play an important role in expanding the preferred spawning habitat. Sardine data in 0604EN and 0704LN are also supportive of the hypothesis. With the broadest area of positive curl in 0604EN and the strongest equatorward wind stress in 0704LN, sardine eggs were sampled far offshore ($> 200 \text{ km}$). Thus, the results support the first hypothesis that wind-forcing modulates the oceanic processes such as transport and temperature field, which affect the spawning habitat.

5. Quality of Spawning Habitat

5.1. Statistical Spawning Habitat Model

[32] Using either CalCOFI or ROMS data, the statistical model predicted that there would be more high quality habitat in 0304EN and 0604EN, which is consistent with the observations showing higher egg densities (more than 100 eggs m^{-3}) in those years (Figure 8). Figure 8 shows the probability of occurrence of Pacific sardine eggs in 0204LN, 0304EN, 0604EN and 0704LN. Spawning habitat model predictions using the CalCOFI surveys (Figure 8, left) clearly show higher probability of occurrence of eggs in the SCB during 0304EN and 0604EN with maximum values higher than 0.5, indicating that the quality of spawning

habitat was better in those periods. The predictions using the ROMS data set (Figure 8, right) also show higher probability of occurrence of eggs in the SCB in 0304EN and 0604EN, which is consistent with the predictions generated from the CalCOFI data.

[33] Furthermore, high quality habitat was also predicted nearshore off central California to the north of the core CalCOFI sampling area in 0304EN and 0604EN. In 0304EN, this was associated with higher egg densities (Figure 1f) and corresponded to higher daily egg production. In 0604EN, however, only a small number of sardine eggs ($< 10 \text{ eggs m}^{-3}$) were sampled there. It is inferred from this that predictions of high quality spawning habitat reflect the potential spawning habitat rather than the actual spawning habitat that will be used by the adult sardine in any given year.

5.2. Convergence of the Water

[34] The convergence of water can partially explain high egg concentrations. Once the spawning occurs, sardine eggs can drift along with the current. During the approximately 3 days between spawning and hatching (the time to hatching is temperature-dependent), eggs can be transported up to 75 km by a current of 0.3 m s^{-1} and redistributed within that range. The sardine eggs are buoyant and floating near the surface, hence it is plausible to find higher concentration of eggs at convergence areas.

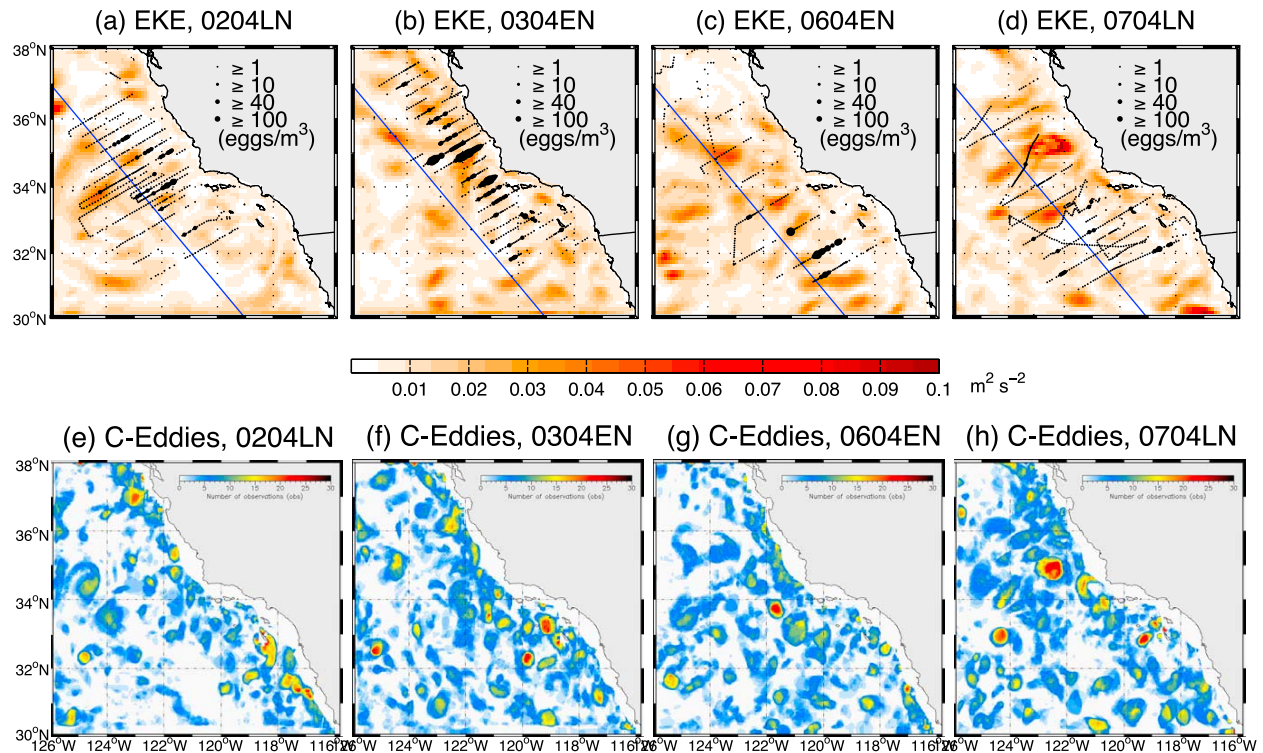


Figure 10. The (a–d) eddy kinetic energy and (e–h) number of cyclonic eddies in 0204LN, 0304EN, 0604EN and 0704LN. Blue lines in Figures 10a–10d that is approximately 300 km from the coast separate inshore and offshore areas. Cyclonic eddies are determined from daily geostrophic currents estimated using the ROMS model. Colors represent numbers of observations above a threshold for the Okubo-Weiss parameter calculated for currents with anti-clockwise rotation.

[35] Velocity potential, which is indicative of convergence and divergence, is computed using the monthly mean surface current, and is shown with egg counts for the states with more than 10 eggs m^{-3} in Figure 9. The velocity potential is the integration of the velocity, and it can be calculated by solving the minimization problem discussed by *Li et al.* [2006]. The scatterplot shows that more stations with high egg concentration have positive velocity potential, suggesting that higher concentration of eggs can be found in the convergence regions. The number of stations with positive velocity potential (159) is more than twice as large as the one with negative velocity potential (69), and the mean of velocity potential is $0.68 \times 10^{-5} \text{ m}^2 \text{ s}$. If the stations with more than 40 eggs m^{-3} are considered, 42 stations have positive velocity potential while only 10 stations with negative values. Thus it is plausible that the convergence of the water can be linked with the high number of the sardine eggs. In addition to the statistical model results, these results are consistent with the second hypothesis that spawning habitat quality is strongly affected by physical properties of the water.

6. Survivor Habitat

[36] Cyclonic mesoscale eddies can increase primary production by pumping up the subsurface nutrient-rich

water. In the same context, cyclonic mesoscale eddies are thought to play an important role in Pacific sardine larval distributions [*Logerwell and Smith, 2001; Auad et al., 2006*]. In this analysis, the EKE was computed from the anomaly of meridional (u) and zonal (v) geostrophic currents components. The anomaly components u' and v' were computed from the SSH anomaly with respect to the 5-year mean from the model data [*Gill, 1982, chapter 7*]. The spatial pattern of EKE in 0204LN and 0304EN is quite different (Figures 10a and 10b). The mean EKE inshore of 300 km from the coast is higher in 0304EN, and the mean offshore EKE is higher in 0204LN (Table 2). However, the pattern is opposite in 0604EN and 0704LN (Figures 10c and 10d and Table 2).

[37] EKE does not reveal the rotational direction of eddies. *Logerwell and Smith* [2001] have shown that growth rates of

Table 2. Spatial Mean EKE ($\times 10^{-3} \text{ m}^2 \text{ s}^{-2}$) as Computed From the Data Assimilation Fits, for Offshore Areas and Inshore Areas

	Mean EKE	Mean Offshore EKE	Mean Inshore EKE
0204LN	7.87	9.08	6.89
0304EN	9.55	8.42	10.44
0604EN	9.56	10.34	8.95
0704LN	9.47	8.42	10.29

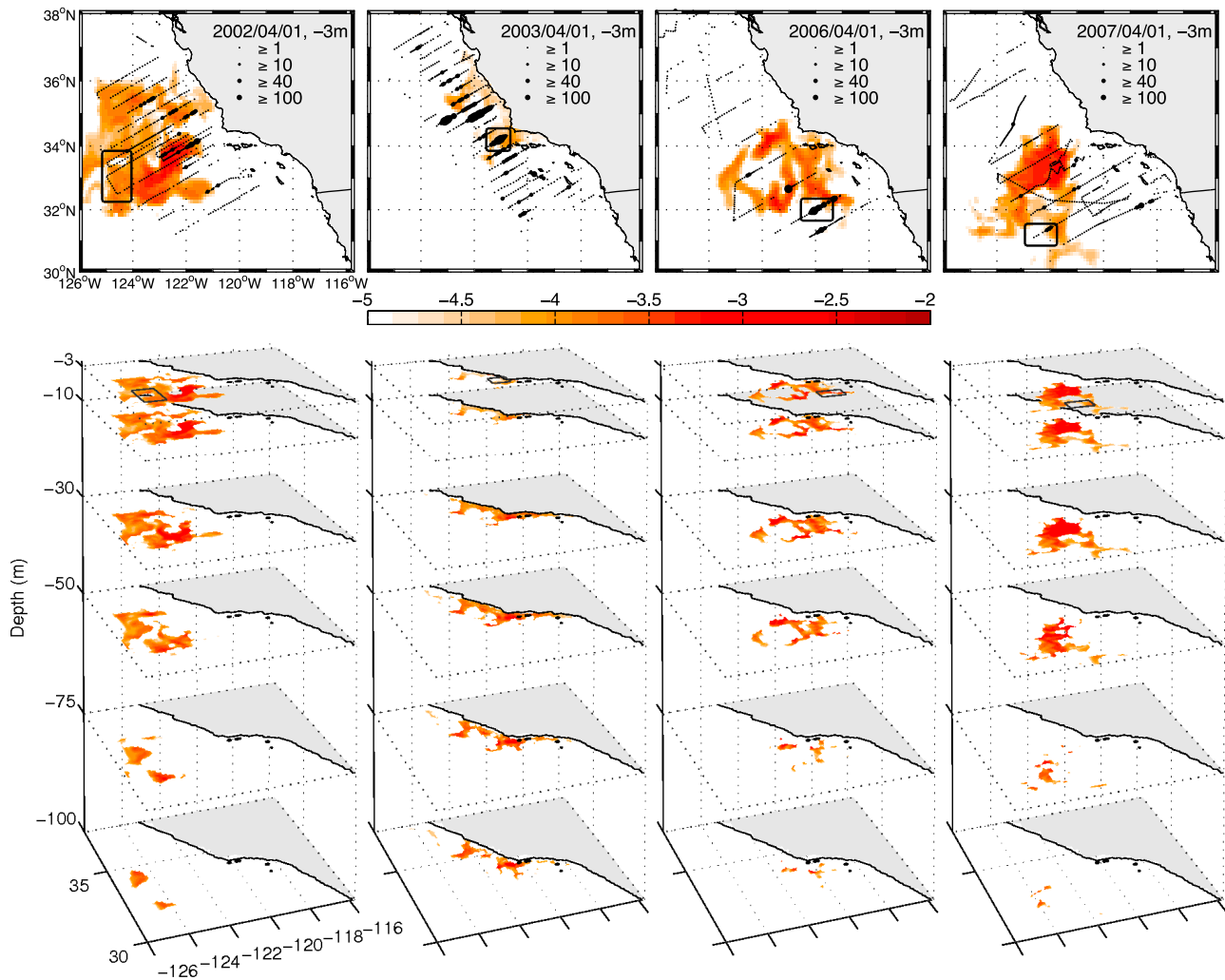
Log₁₀ normalized passive tracer concentration

Figure 11. Results of the one month ROMS adjoint model experiments (top) at -3 m with 2-dimensional view and (bottom) at -3 m, -10 m, -30 m, -50 m, -75 m and -100 m with 3-dimensional view on April 1st of 2002, 2003, 2006 and 2007. Colors represent the normalized sensitivity of passive tracer concentration in \log_{10} scale. Passive tracers were injected in the black squares at upper 10 m on April 30th. Black dots represent the Pacific sardine egg concentration in eggs m^{-3} .

sardine larvae in cyclonic eddies should be an order of magnitude greater than outside these eddies. It is because doming isopycnals bring nutrients into the euphotic zone and this favors increased phytoplankton production. Enhanced primary production provides a suitable environment for production of copepod nauplii (young stages) that are a primary prey of sardine larvae. For this reason cyclonic eddies are referred to as “survivor habitat” [Logerwell *et al.*, 2001] as opposed to spawning habitat where eggs are produced, because the sardine larvae in these eddies are expected to grow faster and survive longer.

[38] The eddy detection was computed using the Okubo-Weiss parameter, and the cyclonic eddies classification was made automatically considering the direction of the currents rotation. The concept that cyclonic eddies constitute sardine

larval survivor habitat is really still an untested hypothesis. This topic is examined only to the point of determining whether postulated survivor habitat differs between 0204LN-0304EN and 0604EN-0704LN, and whether any pattern is consistent with the observed differences in spawning habitat and environmental conditions in the those years. Explicit testing of the hypothesis is the subject of other current work. It is found that cyclonic eddies are more frequent in 0304EN (2.7 counts per 100 km^{-2}) than in 0204LN (2.2 counts per 100 km^{-2}) (Figures 10e and 10f).

[39] Cyclonic eddies are more intense in the SCB in 0304EN, and a greater area between San Francisco and northern Baja California is covered by cyclonic eddies in 0304EN. Thus higher number of cyclonic eddies in 0304EN may infer that the postulated survivor habitat for sardine

Table 3. Mixed Layer (ML) Depth Averaged Over Model Domain and Percentage (%) of the Passive Tracer That Remained in the Domain on April 1st of 2002, 2003, 2006 and 2007^a

	Total (%)	Mean ML Depth (m)	Above ML (%)	Below ML (%)
0204LN	98.89	-14.93	52.21	46.68
0304EN	99.60	-12.16	7.54	92.06
0604EN	99.16	-11.03	32.07	67.09
0704LN	98.28	-34.40	89.56	8.72

^aThe initial perturbation was set up in the black square in Figure 11 on April 30th of each year. The percentage of the passive tracer in the ML and below ML are also computed.

larvae was better than in 0204LN. In 0604EN more cyclonic eddies are located to the south of the Point Conception, suggesting better survivor habitat at the SCB (Figure 10g). Although more cyclonic eddies are detected at central California than the SCB in 0704LN (Figure 10h), it is difficult to link the survivor habitat and the cyclonic eddies because of the lack of the dense sardine eggs sampling. Thus, although the analysis about mesoscale features provide some support for their link to survivor habitat, a lack of information limits the full test of the third hypothesis.

7. Source Waters

[40] As discussed in section 3.1, the adjoint model with a passive tracer can not only identify the location for source waters for the area of interest, but also quantify the relative contribution of the source waters. Hence it is useful to diagnose the source waters and their properties for the areas where high contrast in sardine egg distribution is shown. The initial condition for the adjoint model is the passive tracer concentration from the surface down to -10 m in the area of interest on April 30th. The adjoint model integrates the initial condition backward in time for 30 days and quantifies the source waters to that area. Although the timescale of the adjoint model run is much longer than the sardine egg lifespan (<3 days), identifying the source waters is useful to explain the water properties that can be linked to the sardine egg distribution.

[41] Figure 11 shows the normalized sensitivity of tracer concentration from the adjoint model. The sensitivity is normalized by the total passive tracer concentration and expressed in log₁₀ scale. If the sensitivity in log₁₀ scale at a certain grid point is -2, a perturbation of 1 at that grid point can induce a perturbation of 10⁻² or 1% changes in total passive tracer concentration summed over the area of interest. In general, the areas with higher saturation in color can be interpreted as those areas that are more responsible as the sources. Bottom panels in Figure 11 show the source waters in 3-dimensional view, which is useful to diagnose the depth of the source waters as well as the horizontal distribution of sources at each level.

[42] The relative contribution of source waters is quantified in Table 3. During the one month run of the adjoint model, some portion of passive tracer left the domain, representing the contribution of the source waters from outside of the model domain. Thus, the percentage of the total passive tracer remained in the model domain is first

calculated. Then the mixed layer depth is estimated using the density with threshold value of 0.03 kg m⁻³ [de Boyer Montégut et al., 2004], and the contribution from the mixed layer and outside of the mixed layer are quantified for each period. The maximum mean mixed layer depth was observed in 0704LN when the wind stress is the maximum.

[43] In 0204LN and 0704LN, the area of interest marked by black squares are selected around the offshore CUFES stations to verify that transport is one of the responsible mechanism for broad sardine egg distribution. The source waters can be found mostly from inshore areas in 0204LN. More than 98% of the initial passive tracer remains in the model domain, even though the black square is close to the western boundary (Table 3). In addition, the sardine eggs were observed in the source waters, indicating that the source water properties are favorable for sardine spawning. In 0704LN, the source waters can be found mostly from the north of the black square, indicating the equatorward flow carries source waters (Figure 5d). Sardine eggs were also sampled in the source waters, implying that the properties of source waters are spawning favorable.

[44] The passive tracer is also found subsurface below the mixed layer on April 1st in both 0204LN and 0704LN, though the contribution of the water below mixed layer to the areas of interest is less than the surface water (Table 3). The adjoint model reveals that the water deeper than -100 m is lifted to the upper layer (>-10 m) in one month. In 0304EN and 0604EN, however, the upwelling cells are shallower than -70 m when the initial passive tracers in 0304EN and 0604EN are released at the same areas as in 0204LN and 0704LN, respectively (now shown). This supports the idea that the supply of nutrient rich water from subsurface to surface contributes to make offshore areas good for spawning in 0204LN and 0704LN. Note that the offshore upwelling is related either to divergence of the surface water or vertical diffusion instead of wind-forcing because the wind stress curl is not positive (Figure 4).

[45] Areas with high concentration of sampled eggs are chosen as areas of interest in 0304EN and 0604EN. The areas marked with black squares show more than 100 eggs m⁻³ in both periods. In 0304EN, upwelling is the primary mechanism to bring the subsurface water to the area marked with black square and make the water spawning favorable. The upwelling speed is greater than 3 m day⁻¹ because water deeper than -100 m is brought up to the surface in 30 days. More than 92% of the total passive tracer comes from subsurface (Table 3), indicating a majority of source waters coming from subsurface. The source can also be found at the surface near the coast from both the north and the south where high levels of Chl-*a* occur (Figure 2b).

[46] In 0604EN, the passive tracer patches on April 1st are generally distributed in the northwestern part of the black square including the coastal areas near Point Conception, reflecting the equatorward California Current. As seen in Figure 2c, Chl-*a* level is high (>√10 mg m⁻³) at source water regions, especially the south of Point Conception. Thus, nutrient rich water is supplied to the area marked with black square in 0604EN. Subsurface water also contributes more than 67% of the total passive tracer. The upwelling is related with wind-forcing because positive value of wind stress curl can induce the Ekman pumping upwelling. Thus,

the adjoint model results support the hypotheses regarding the spawning habitat area and its quality.

8. Summary and Discussion

[47] The California Current System (CCS) experienced dramatic changes during the transition from the 2002 La Niña to the 2003 El Niño and from the 2006 El Niño to the 2007 La Niña. Equatorward upwelling favorable wind was stronger than normal in April 2002 (0204LN) and 2007 (0704LN) and a negative sea surface temperature (SST) anomaly was observed. During April 2003 (0304EN) and 2006 (0604EN), upwelling favorable wind was weakened, resulting in a positive SST anomaly.

[48] Such abrupt environmental changes can affect the ecosystem significantly. The Pacific sardine egg data sampled by CUFES showed sharply different patterns in horizontal distribution and concentration in 0204LN and 0304EN. The sardine eggs were found over a broader area offshore in 0204LN while eggs did not extend nearly as far offshore in 0304EN (Figure 1). The contrast in the sampled eggs data during 0604EN-0704LN transition was not as evident as in 0204LN-0304EN, but the concentration of eggs show the same pattern of change.

[49] In order to investigate the physical processes associated with the horizontal patterns of Pacific sardine eggs, the physical ocean states were prepared using the ROMS simulations and the 4DVAR data assimilation system. The fits assimilated SSH, SST and hydrographic temperature and salinity data for 0204LN, 0304EN, 0604EN and 0704LN. The data assimilation using the ROMS 4DVAR system provided the dynamically consistent physical ocean states as well as the adjusted atmospheric surface forcing to interpret these conditions. The adjoint model runs with passive tracer identified the source waters for key areas of interest to sardine spawning.

[50] Anomalously strong equatorward wind-forcing drove stronger offshore transport, resulting in offshore expansion of sardine spawning habitat in 0204LN. *Schwing et al.* [2002a] also pointed out upwelling filaments and relatively high surface chlorophyll-*a* concentration were the two main causes for the sardine eggs found offshore in 0204LN. The SST pattern was modulated by wind-forcing through upwelling and offshore transport, and played a role as one of the most important determining factors for spawning habitat. The statistical spawning habitat model and convergence of water can partially explain the observed high egg concentrations in 0304EN and 0604EN. Mesoscale eddy fields suggest that the physical oceanic conditions in 0304EN provided more preferable larvae survivor habitat than in 0204LN. The source waters revealed the importance of transport for the extension of spawning area in 0204LN and 0704LN, and the water for the areas with high egg concentration in 0304EN and 0604EN was provided from nutrient-rich sources.

[51] In summary, the “broadening” or “extension” of preferred spawning habitat offshore due to increased wind-driven offshore transport was seen in 0204LN and 0704LN under La Niña conditions. In 0304EN under El Niño conditions, the preferred spawning habitat was not as broad as in other periods, but the quality of the spawning habitat and larvae survivor habitat was better. Good quality of spawning

habitat was predicted in 0604EN, but the spawning habitat was not limited to the regions near the coastal areas, partially due to the open water upwelling.

[52] There are, however, still many unknown factors that can control the sardine egg distribution. Sampling timing is an important factor to affect the observed distribution of eggs. CUFES April surveys are not necessarily executed at the peak spawning period. In some years, spawning can happen early spring while it happens late spring in other years. Thus the total egg number and the concentration of eggs can be different if the sampling misses the peak of spawning. The limitation in the spatial coverage of the cruise can change the apparent horizontal distribution as well. In 0204LN and 0704LN, for example, the areas with temperature between 12.5°C and 15°C extended further offshore beyond the western limits of the transects. Thus it is plausible that more eggs could be sampled if the cruise had gone further to the west, and this eventually affects the total number of sampled eggs. The coverage of the CUFES cruises for central California in 0604EN and 0704LN is not as dense as for other two years, leaving the possibility that more sardine eggs could have been sampled.

[53] Note that the biological communities do not respond in the same way to each El Niño - La Niña transition. As seen in this study, the responses of the sardine spawning habitat are not the same between 0204LN-0304EN and 0604EN-0704LN. In the 1997/99 transition, there was a huge shift toward sub-tropical communities in the SCB due to advective processes [*Chavez et al.*, 2002; *Checkley and Barth*, 2009; *Lea and Rosenblatt*, 2000], but advection of water masses was less apparent in 2009/2010 [*Todd et al.*, 2011]. Thus the sardine egg distribution may differ between ENSO transitions because the factors controlling sardine spawning behavior are not fully understood.

[54] Nonetheless, the physical model alone can be useful to understand the link between the observed interannual variance of the sardine spawning, and the variance of basin scale atmospheric forcing and the oceanic responses. The adjoint model with a passive tracer also is beneficial for identifying the source waters and its properties for the sardine spawning areas. These dynamically consistent physical ocean states can now provide the basis for running ecosystem models during these time periods to better represent lower trophic level response to changing physical ocean conditions. This aspect of the response will be explored in future work.

[55] **Acknowledgments.** This study formed a part of the Ph.D. dissertation of HS at Scripps Institution of Oceanography. Funding was provided by NSF (CCE-LTER: OCE-0417616 and OCE-1026607) and NOAA (IOOS: NA17RJ1231). Postdoctoral salaries for EDW and KMN were funded by NOAA (IOOS: NA17RJ1231). SM was supported by NOAA Fisheries And The Environment program (FATE). The views expressed herein are those of the authors and do not necessarily reflect the views of NOAA or any of its subagencies. Supercomputing resources were provided by COMPAS at SIO. Argo data were collected and made freely available by the International Argo Project and the national programs that contribute to it. (<http://www.argo.ucsd.edu>, <http://argo.jcommops.org>). Argo is a pilot program of the Global Ocean Observing System. The authors would like to thank two anonymous reviewers for valuable comments and suggestions.

References

Auad, G., A. J. Miller, and E. D. Lorenzo (2006), Long-term forecast of oceanic conditions off California and their biological implications, *J. Geophys. Res.*, *111*, C09008, doi:10.1029/2005JC003219.

- Bjorkstedt, E., et al. (2010), State of the California Current 2009–2010: Regional variation persists through transition from La Niña to El Niño (and back?), *Rep.* 51, pp. 39–69, Calif. Coop. Oceanic Fish. Invest., La Jolla.
- Broquet, G., C. A. Edwards, A. M. Moore, B. S. Powell, M. Veneziani, and J. D. Doyle (2009), Application of 4D-Variational data assimilation to the California Current System, *Dyn. Atmos. Oceans*, 48, 69–92.
- Chavez, F., C. Collins, A. Huyer, and D. Mackas (2002), El niño along the west coast of North America, *Prog. Oceanogr.*, 54, 1–6.
- Checkley, D. M., Jr., and J. A. Barth (2009), Patterns and processes in the California Current System, *Prog. Oceanogr.*, 83, 49–64.
- Checkley, D. M., Jr., P. B. Ortner, L. R. Settle, and S. R. Cummings (1997), A continuous, underway fish egg sampler, *Fish. Oceanogr.*, 6, 58–73.
- Checkley, D. M., Jr., R. C. Dotson, and D. A. Griffith (2000), Continuous, underway sampling of eggs of Pacific sardine (*Sardinops sagax*) and northern anchovy (*Engraulis mordax*) in spring 1996 and 1997 off southern and central California, *Deep Sea Res.*, 47, 1139–1155.
- Chhak, K., and E. Di Lorenzo (2007), Decadal variations in the California Current upwelling cells, *Geophys. Res. Lett.*, 34, L14604, doi:10.1029/2007GL030203.
- de Boyer Montégut, C., G. Madec, A. S. Fischer, A. Lazar, and D. Iudicone (2004), Mixed layer depth over the global ocean: An examination of profile data and a profile-based climatology, *J. Geophys. Res.*, 109, C12003, doi:10.1029/2004JC002378.
- Doyle, J. D., Q. Jiang, Y. Chao, and J. Farrara (2009), High-resolution real-time modeling of the marine atmospheric boundary layer in support of the AOSN-II field campaign, *Deep Sea Res., Part II*, 56, 87–99.
- Fairall, C. W., E. F. Bradley, D. P. Rogers, J. B. Edson, and G. S. Young (1996), Bulk parameterization of air-sea fluxes for TOGA COARE, *J. Geophys. Res.*, 101, 3747–3767.
- Fukumori, I., T. Lee, B. Cheng, and D. Menemenlis (2004), The origin, pathway, and destination of Niño-3 water estimated by a simulated passive tracer and its adjoint, *J. Phys. Oceanogr.*, 34, 582–604.
- Ghil, M., and P. Malanotte-Rizzoli (1991), Data assimilation in meteorology and oceanography, *Adv. Geophys.*, 33, 141–266.
- Gill, A. E. (1982), *Atmosphere-Ocean Dynamics*, 662 pp., Academic, San Diego, Calif.
- Goericke, R., et al. (2007), The state of the California current, 2006–2007: Regional and local processes dominate, *Rep.* 48, pp. 33–66, Calif. Coop. Oceanic Fish. Invest., La Jolla.
- Hodur, R. M., J. Pullen, J. Cummings, X. Hong, J. Doyle, P. Martin, and M. Rennick (2002), The coupled ocean/atmosphere mesoscale prediction system (COAMPS), *Oceanography*, 15, 88–98.
- Lea, R., and R. Rosenblatt (2000), Observations on fishes associated with the 1997–98 El Niño off California, *Rep.* 41, pp. 117–129, Calif. Coop. Oceanic Fish. Invest., La Jolla.
- Le Dimet, F., and O. Talagrand (1986), Variational algorithms for analysis and assimilation of meteorological observations: Theoretical aspects, *Tellus, Ser. A*, 38, 97–110.
- Li, Z., Y. Chao, and J. C. McWilliams (2006), Computation of the streamfunction and velocity potential for limited and irregular domains, *Mon. Weather Rev.*, 134, 3384–3394.
- Lo, N. C. H., Y. A. G. Ruiz, M. J. Cervantes, H. G. Moser, and R. J. Lynn (1996), Egg production and spawning biomass of Pacific sardine (*Sardinops sagax*) in 1994, determined by the daily egg production method, *Rep.* 37, pp. 160–174, Calif. Coop. Oceanic Fish. Invest., La Jolla.
- Lo, N. C. H., B. J. Macewicz, and D. A. Griffith (2005), Spawning biomass of Pacific sardine (*Sardinops sagax*), from 1994–2004 off California, *Rep.* 46, pp. 93–112, Calif. Coop. Oceanic Fish. Invest., La Jolla.
- Logerwell, E. A., and P. E. Smith (2001), Mesoscale eddies and survival of late stage Pacific sardine (*Sardinops sagax*) larvae, *Fish. Oceanogr.*, 10, 13–25.
- Logerwell, E., B. Lavaniegos, and P. Smith (2001), Spatially-explicit bioenergetics of Pacific sardine in the Southern California Bight: Are mesoscale eddies areas of exceptional production?, *Prog. Oceanogr.*, 49, 391–406.
- McClatchie, S., et al. (2008), The state of the California current, 2007–2008: La Niña conditions and their effects on the ecosystem, *Rep.* 49, pp. 39–76, Calif. Coop. Oceanic Fish. Invest., La Jolla.
- Miller, A., F. Chai, S. Chiba, J. Moisan, and D. Neilson (2004), Decadal-scale climate and ecosystem interactions in the North Pacific Ocean, *J. Oceanogr.*, 60, 163–188.
- Moore, A. M., H. G. Arango, G. Broquet, B. S. Powell, J. Zavala-Garay, and A. T. Weaver (2011), The Regional Ocean Modeling System (ROMS) 4-dimensional variational data assimilation systems, part I: Formulation and overview, *Prog. Oceanogr.*, 91, 34–49.
- Peterson, W. T., et al. (2006), The state of the California current, 2005–2006: Warm in the north, cold in the south, *Rep.* 47, pp. 30–74, Calif. Coop. Oceanic Fish. Invest., La Jolla.
- Reiss, C. S., D. M. Checkley Jr., and S. J. Bograd (2008), Remotely sensed spawning habitat of Pacific sardine (*Sardinops sagax*) and northern anchovy (*Engraulis mordax*) within the California Current, *Fish. Oceanogr.*, 17, 126–136.
- Rykaczewski, R. R., and D. M. Checkley Jr. (2008), Influence of ocean winds on the pelagic ecosystem in upwelling regions, *Proc. Natl. Acad. Sci.*, 105(6), 1965–1970.
- Schwing, F. B., T. Murphree, L. deWitt, and P. M. Green (2002a), The evolution of oceanic and atmospheric anomalies in the northeast Pacific during the El Niño and La Niña events of 1995–2001, *Prog. Oceanogr.*, 54, 459–491.
- Schwing, F. B., et al. (2002b), The state of the California Current, 2001–2002: Will the California Current System keep its cool, or is El Niño looming?, *Rep.* 43, pp. 31–68, Calif. Coop. Oceanic Fish. Invest., La Jolla.
- Schwing, F. B., N. A. Bond, S. J. Bograd, T. Mitchell, M. A. Alexander, and N. Mantua (2006), Delayed coastal upwelling along the U.S. west coast in 2005: A historical perspective, *Geophys. Res. Lett.*, 33, L22S01, doi:10.1029/2006GL026911.
- Sherman, J., R. E. Davis, W. B. Owens, and J. Valdes (2001), The autonomous underwater glider “Spray,” *IEEE J. Oceanic Eng.*, 26(4), 437–446.
- Singh, A., T. Delcroix, and S. Cravatte (2011), Contrasting the flavors of El Niño–Southern Oscillation using sea surface salinity observations, *J. Geophys. Res.*, 116, C06016, doi:10.1029/2010JC006862.
- Song, H. (2011), Sensitivity analysis, ocean state estimation and diagnostics in the California Current, PhD dissertation, 165 pp., Univ. of Calif., San Diego, La Jolla.
- Song, H., A. J. Miller, B. D. Cornuelle, and E. Di Lorenzo (2011), Changes in upwelling and its water sources in the California Current System driven by different wind forcing, *Dyn. Atmos. Oceans*, 52, 170–191.
- Todd, R. E., D. Rudnick, R. Davis, and M. Ohman (2011), Underwater gliders reveal rapid arrival of El Niño effects off California’s coast, *Geophys. Res. Lett.*, 38, L03609, doi:10.1029/2010GL046376.
- Venrick, E., et al. (2003), The state of the California Current, 2002–2003: Tropical and subarctic influences vie for dominance, *Rep.* 44, pp. 28–60, Calif. Coop. Oceanic Fish. Invest., La Jolla.
- Weber, E. D., and S. McClatchie (2010), Predictive models of northern anchovy *Engraulis mordax* and Pacific sardine *Sardinops sagax* spawning habitat in the California Current, *Mar. Ecol. Prog. Ser.*, 406, 251–263.
- D. M. Checkley Jr. and A. J. Miller, Scripps Institution of Oceanography, University of California, San Diego, La Jolla, CA 92093, USA.
- S. McClatchie, K. M. Nieto, and E. D. Weber, Southwest Fisheries Science Center, NOAA, 8604 La Jolla Shores Dr., La Jolla, CA 92037-1508, USA.
- H. Song, Department of Ocean Sciences, University of California, Santa Cruz, CA 95064, USA. (hsong6@ucsc.edu)